Effects of Densely Sampled Dipole Field on Quantitative Susceptibility Mapping

Yuya Umemoto, Mai Murashima, Tomohiro Ueno-*IEEE Member,* and Naozo Sugimoto

Abstract— **We present a method of resolving a fine structure in a magnetic susceptibility map, which cannot be distinguished by the conventional method, by using a densely sampled dipole field and by expanding a magnetic field perturbation map. We investigate effects of a sampling density of the dipole field on the spatial resolution and on obtained susceptibility values. When the sampling density is increased, a shape of an otherwise undistinguishable fine structure recovers gradually in an obtained susceptibility map. Furthermore, a peak susceptibility value of the fine structure is slowly getting closer to the correct values.**

I. Introduction

Unusual accumulation of iron is found in a histological brain section of neurodegenerative disease such as Parkinson's disease[1] and Alzheimer's disease[2]. Since iron is a ferromagnetic material, iron accumulation strongly enhances local tissue magnetic susceptibility in a brain. Thus, iron deposits can be assessed by measuring the magnetic susceptibility. If the tissue magnetic susceptibility can be quantified, progression of the neurodegenerative diseases can be diagnosed in a quantitative manner. Furthermore, earlier diagnosis will be possible if the tissue magnetic susceptibility can be evaluated in a smaller region.

In order to quantitatively obtain a spatial distribution of local tissue magnetic susceptibility, a new technique of MRI, Quantitative Susceptibility Mapping(QSM), has been developed. Under a static external magnetic field, local magnetization, which is proportional to the local tissue magnetic susceptibility, induces dipole fields to surrounding tissues. In MRI, nuclear spins precess about a local magnetic field, which is a sum of the external magnetic fields and magnetic field perturbations. The magnetic field perturbations are integration of dipole fields from a whole space and can be measured as phase data of gradient echoes. Therefore, in QSM, a magnetic susceptibility distribution is calculated by solving nonlocal inverse problem of magnetic field perturbations. Since a Fourier transformed dipole field has zero values on two conical surfaces, direct inversion is prohibited in QSM[3]. To deal with this ill-posed nature of the inverse problem, several methods have been proposed such as regularization methods[4] and multiple orientation methods[5][6].

In addition to that it has zero values on the conical surface in k-space, the dipole field has a rapid changing nature. The dipole field decays with the cube of the distance from the origin, and changes its sign according to its direction. Therefore, a large change within a small region exists near the origin of the dipole field. This rapid changing nature also appears in k-space as a Fourier transformed dipole field does not decay even at high k value. If a digitally sampled unit dipole field is used in QSM, discrepancy from the continuous one brings errors to a calculated magnetic susceptibility map[7][8]. Moreover, due to limitation of an MRI hardware, measured magnetic field perturbations include unavoidable partial volume effects. As a result, the calculated magnetic susceptibility distribution loses fine details of its structure and susceptibility values. The rapid changing nature of the dipole field and the partial volume effects of the measured magnetic field perturbations complicate the ill-posed inverse problem of QSM.

Although the measured magnetic field perturbation cannot be resolved into smaller structures than a spatial resolution, the dipole field can be calculated in an infinitesimal scale. We have proposed to use a densely sampled dipole field for improving a spatial resolution of a magnetic susceptibility map. And we have confirmed that a fine structure, which the conventional method cannot resolve, becomes distinguishable by using a three times densely sampled dipole field[9]. Here, we investigate dependences of shapes of smaller structures and of susceptibility values on a sampling density of a dipole field in our proposed method by performing simulations with a 3D Shepp-Logan phantom including partial volume effects.

II. Methods

We created a 3D Image of $(24)^3$ voxels including partial volume effects and used as MRI input data. In the following sections, we define matrix size of a 3D Image with n times higher sampling density as $(24\times n)^3$. And the multiplicative n is defined as a scaling factor. When we enlarge FOV of the 3D Image in m times, the matrix size will be written as $(24\times n\times m)^3$.

A. Magnetic Field Perturbation Map Including Partial Volume Effects

A high resolution 3D Shepp-Logan phantom was created at the matrix size of $(24\times 9)^3$. There were seven prolate spheroids (regions 1~4 and 8~10) and three spheres (regions

Y. Umemoto was with the Human Health Science, Faculty of Medicine, Kyoto University, Kyoto, Kyoto 606-8507 Japan. He is with Human Health Science, Graduate School of Medicine, Kyoto University, Kyoto, Kyoto 606-8507 Japan (corresponding author to provide phone: +81-75-751-3934; fax: +81-75-751-3909; e-mail: umemoto.yuya.26z@st.kyoto-u.ac.jp).

M. Murashima was with the Human Health Science, Graduate School of Medicine, Kyoto University, Kyoto, Kyoto 606-8507 Japan. She is now with Toshiba Medical Systems Corporation, Otawara-shi, Tochigi-ken 324-0036, Japan (e-mail: mmura1026@gmail.com).

T. Ueno and N. Sugimoto are with the Human Health Science, Graduate School of Medicine, Kyoto University, Kyoto, Kyoto 606-8507 Japan (e-mail: ueno.tomohiro.2u@kyoto-u.ac.jp; sugimoto.naozo.8x@kyoto-u.ac.jp).

978-1-4244-7929-0/14/$26.00 ©2014 IEEE

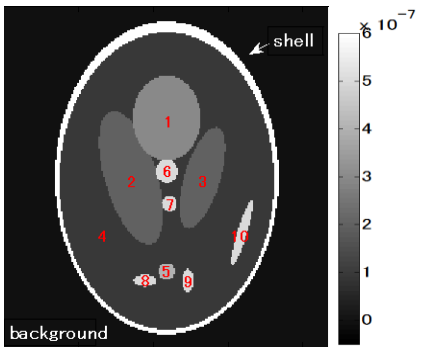

Fig.1. Center slice (z=109) of a high resolution 3D Shepp-Logan phantom at matrix size of $(24\times9)^3$. There are ten regions, where each magnetic susceptibility (χ_i) is: χ_1=0.3; χ_2=0.2; χ_3=0.2; χ_4=0.1; χ_5=0.4; $\chi_{6\sim10}$=0.5; χ_{shell}=1.0; χ_{BG}=0 ppm.

5~7) inside an outer shell of the region 4 as shown in Fig.1. Unlike an ordinary Shepp-Logan phantom, we added extra small regions which could not be detected with a low spatial resolution. Magnetic susceptibilities of the regions 1~5 ($\chi_1\sim\chi_5$) were set to 0.3, 0.2, 0.2, 0.1 and 0.4 ppm, respectively. Those of the regions 6~10 ($\chi_6\sim\chi_{10}$) were set to 0.5 ppm. The outer shell of the region 4 and the outside of the outer shell (background) was set to 1.0 and 0 ppm respectively.

A general idea of creating a magnetic field perturbation map is same as in [7][8]. In this study, we utilized an analytically derived Fourier transformed dipole field instead of a numerically derived one. Here, the analytically derived Fourier transformed dipole field ($\mathcal{F}\{d_z\}$) is given by

$$\mathcal{F}\{d_z(\vec{k},\theta)\} = \frac{1}{3} - \frac{(k_z\cos\theta - k_y\sin\theta)^2}{|\vec{k}|^2}, \qquad (1)$$

where θ is the angle that z axis of k-space (k_z) makes with respect to a static external magnetic field [6].

The high resolution 3D Shepp-Logan phantom of $(24\times9)^3$ voxels was placed into a central region of a large zero matrix of $(24\times9\times3)^3$ voxels, in order to obtain an enlarged magnetic field perturbation map. Convolution of the enlarged phantom of $(24\times9\times3)^3$ voxels with a dipole field was done in k-space, where the analytically derived Fourier transformed dipole field of $(24\times9\times3)^3$ voxels were used. The central part of the enlarged magnetic field perturbation map was cropped to have a matrix size of $(24\times9)^3$. After replacing to zero value in the region of the outer shell and the background, the cropped magnetic field perturbation map was downscaled to a matrix size of $(24\times1)^3$ by averaging every 9^3 voxels to include partial volume effects. We used the downscaled magnetic field perturbation maps as MRI input data. We prepared three input map sets with different angles (θ) to the static magnetic fields.

B. Susceptibility Estimations by Using Densely Sampled Dipole Fields

In our proposed method, a densely sampled dipole field of $(24\times n)^3$ voxels were employed to obtain a magnetic susceptibility map at the size of $(24\times n)^3$. The input magnetic field perturbation map of $(24\times1)^3$ voxels was interpolated to the size of $(24\times n)^3$ by using the nearest neighbor algorithm so that its high frequency components could be conserved.

A magnetic susceptibility map of a smaller voxel size $(1/n)^3$ was evaluated by deconvoluting the analytically derived densely sampled dipole field of $(24\times n)^3$ voxels from the interpolated magnetic field perturbation map of $(24\times n)^3$ voxels. In this study, eight different scaling factors n=2~9 were used.

In the conventional method, a magnetic susceptibility map was calculated by using scaling factor n=1. In order to have the same voxel size as in the proposed method, the estimated magnetic susceptibility map was interpolated to larger matrix size of $(24\times n)^3$ voxels by using the bicubic algorithm.

C. Susceptibility Estimation

Since our numerical phantom had no susceptibility anisotropy, we employed COSMOS[5] to calculate susceptibility distribution by using three angles (θ), -60°, 0° and 60°. In order to remove a background field, SHARP method[10] was applied. The input magnetic field perturbation map of $(24\times n)^3$ voxels was enlarged to $(24\times n\times2)^3$ voxels by the zero filling. Then, to remove a background field, the enlarged input perturbation map was convolved with a spherical kernel, δ-ρ, which diameter was set to 7 voxels. The deconvolution of the input background removed perturbation map with the dipole field was done in Fourier domain. The analytically derived Fourier transformed dipole field was multiplied by the Fourier transformed spherical kernel $(\mathcal{F}(\delta-\rho))$ in a pointwise manner. The resulted pointwise product was set to zeros in regions where its absolute values were less than 0.14[6]. Susceptibility maps were divided by the pointwise product at each orientation in k-space. Then, the derived susceptibility maps of three angles were averaged in the Fourier domain by weighting their values by the absolute value of the pointwise product for each orientation so that each measurement made an equal contribution. Susceptibility map was evaluated from the weighted mean of the derived susceptibility maps, and was cropped to $(24\times n)^3$ voxels. In this study, all calculations were performed on MATLAB R2013b.

III. Results

A. Comparison of Susceptibility Maps

Fig.2 (a)-(d) shows center slices of trimmed ideal magnetic susceptibility maps of scaling factors, n=1, 2, 4 and 8. The ideal susceptibility maps have been created from the high resolution susceptibility map of $(24\times9)^3$ voxels by resizing the original matrix size to $(n/9)^3$. In order to keep an image resolution, all maps in Fig.2 have been interpolated by using the nearest neighbor algorithm to have a matrix size of $(24\times8)^3$. Although the region 7 cannot be distinguished in the ideal map of the scaling factor n=1 (Fig.2 (a)), it can be identified in those of the scaling factor $n \geqq 2$ (Fig.2 (b)-(d)). It is difficult to extract a spherical shape of the region 7 from the ideal map of the scaling factor n=2, not from those of the scaling factors n=4 and 8.

Fig.2 (e)-(h) shows center slices of susceptibility maps obtained by the conventional method with the scaling factors n=1, 2, 4 and 8. The susceptibility map of the scaling factor

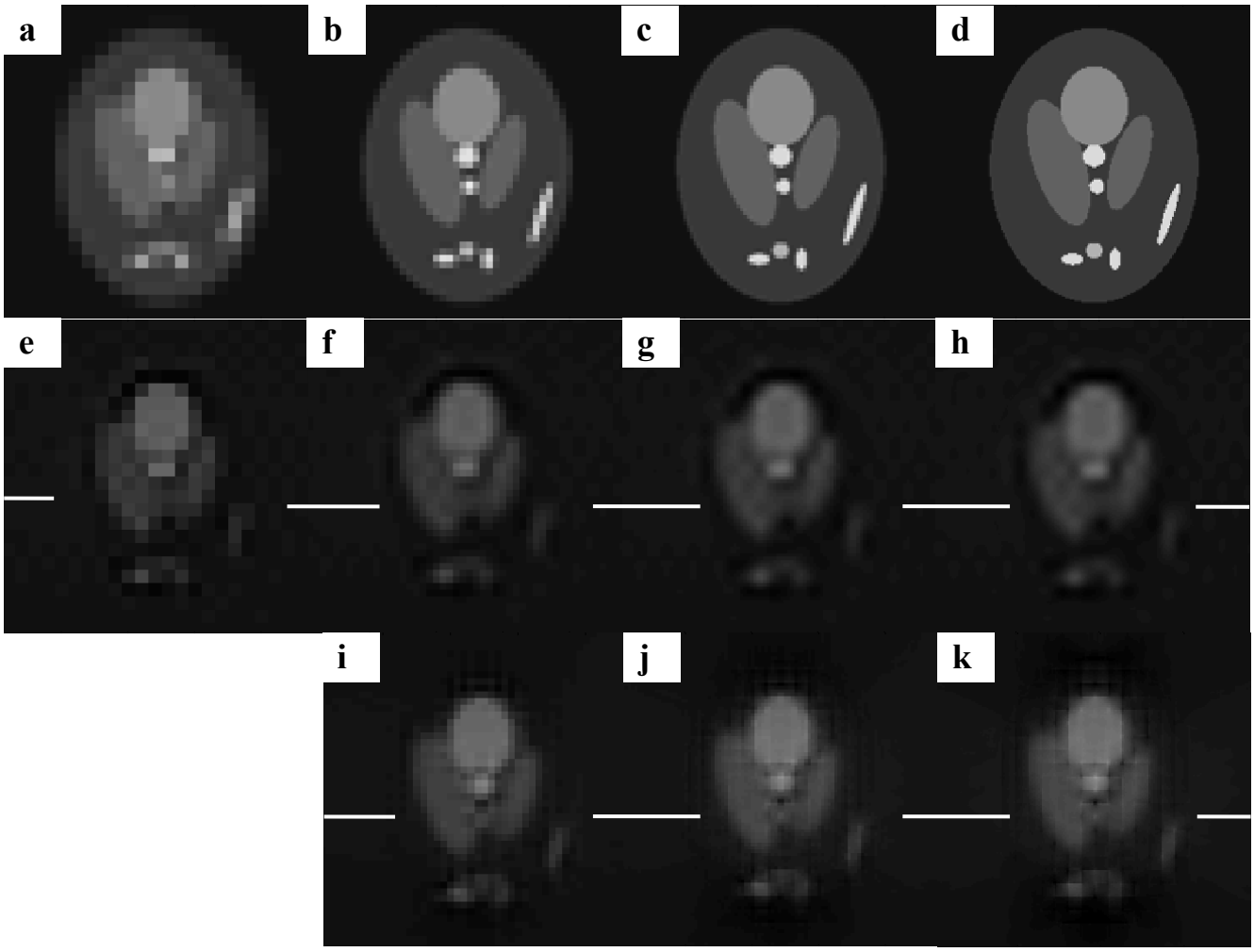

Fig.2. Ideal susceptibility maps and calculated susceptibility maps by the conventional method and by the proposed method. (a)-(d) ideal maps of scaling factors n = 1, 2, 4 and 8; (e)-(h) calculated maps by the conventional method of scaling factors n = 1, 2, 4 and 8; (i)-(k) calculated maps by the proposed method of scaling factors n = 2, 4 and 8. The image size is adjusted to $(24\times8)^3$ voxels, as described in the text.

n=1 reproduced the ideal map of the scaling factor n=1 very well. As the scaling factor is increased, however, only smoothing effects become large. While the region 5 becomes to be identified, the region 7 remains to be merged with the regions 2, 3.

Fig.2 (i)-(k) shows center slices of susceptibility maps obtained by the proposed method with the scaling factor n=2, 4 and 8. In the susceptibility maps of the proposed method, the regions 5, 8 and 9 are distinguishable from each other. Moreover, a boundary of the region 7 appears. As the scaling factor is increased, the shape of each region recovers gradually although the changing rate is much slower than that in the ideal maps. Nevertheless, latticed patterns artifacts exist in all susceptibility maps of the proposed method.

B. Comparison of Susceptibility Profiles

Fig.3 (a)-(c) shows susceptibility profiles at the middle horizontal line in the center slice (as indicated in Fig.2 (e)-(k)) by the both methods with scaling factor n=2, 4 and 8. The red lines corresponds to profiles of the maps of the proposed method and blue lines correspond to those of the conventional method. A calculated susceptibility of the region 4 has been subtracted as a background from each profile in Fig.3. The susceptibility of the region 4 of the scaling factor n=2, 4 and 8 has been determined by averaging obtained values within the region 4 where the flat susceptibility (χ_4=0.1 ppm) is found in

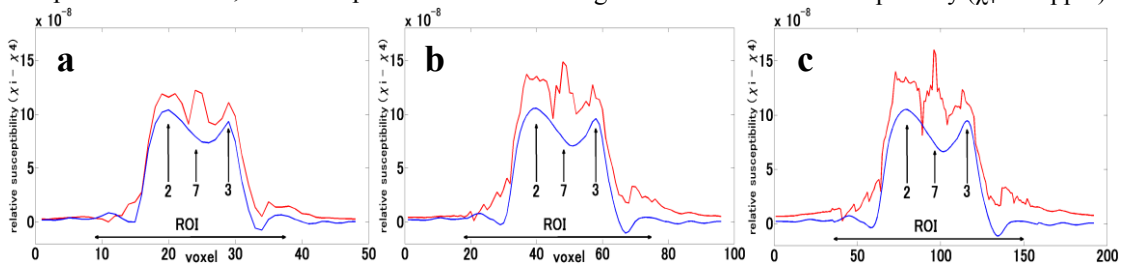

Fig.3. Susceptibility profiles of the proposed method and of the conventional method with scaling factor n=: (a) 2; (b) 4; (c) 8. Red lines correspond to profiles of the proposed method and blue lines correspond to those of the conventional method.

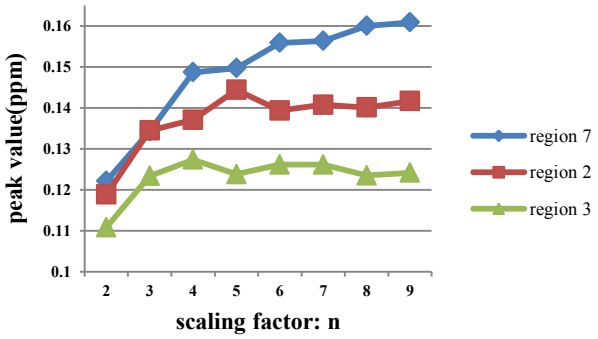

Fig.4. Scaling factor dependence of susceptibility peaks of the center profiles. Blue diamonds, red squares and Green triangles correspond to the peak values of the region 7, 2 and 3.

the ideal maps of scaling factor n=2, 4 and 8 respectively. As appeared in the susceptibility maps, the profiles of the proposed method have trimodal distribution in the central part, which correspond to the region 2, 7 and 3. On the other hand, the ones of the conventional method have only bimodal distribution. As the scaling factor is increased, the peak value of the region 7 of the proposed method increases gradually to the ideal value, while the peak value of the conventional method remains same. Although susceptibility values increase as a whole in the map of the proposed method, the increasing rate of the region 7 is higher than those of other regions.

In Fig.4, we have plotted the peak values of the regions of the center profiles (Fig.3) versus the scaling factor, n. As can be seen, the peak values of the region 2 and 3 are saturated around the scaling factor n=3. On the other hand, the peak value of the region 7 increases even around the scaling factor n=8.

IV. Discussion

The results obtained in this investigation shows that a magnetic susceptibility map can be acquired with a higher spatial resolution than a measured spatial resolution of a magnetic field perturbation map by using a densely sampled dipole field. Moreover, as the scaling factor, n, is increased, small structures and magnetic susceptibility values tend to recover the ideal state.

The resolution improvement by a densely sample dipole field can be qualitatively understood as following. Since the dipole field has the rapid changing nature, a difference of a source position in a subvoxel scale produces a large magnetic field perturbation difference. Therefore, on a deconvolution process, an extra degree of freedom in the source position leads to better findings of a correct position. In addition, the nearest neighbor method in interpolating a measured field perturbation map give equal weight to each subvoxel so that probability of choosing a boundary position as a source position becomes higher than in the case of the bicubic method.

Although the greater resolution improvement was observed in the proposed method by using denser sampling of the dipole field, an obtained susceptibility map did not match with an ideal map with the same resolution even in densest sampling. This may be originated from that due to partial volume effects of a measured perturbation map, some of higher frequency components of a susceptibility map are smeared out and cannot be recovered by denser sampling of the dipole field. Furthermore, the partial volume effects of a measured map may explain why a concentration of a susceptibility value into a small region with a high susceptibility value progresses along with a slower rise of a susceptibility values in a surrounding region, when the scaling factor of a dipole field is increased, as can be seen in Fig. 3, 4. Additional susceptibility value, which is recovered by denser sampling of the dipole field, partially spreads out around a surrounding region due to a partial information loss of the source position by the partial volume effects. Even though the concentration happens more slowly than in the ideal maps, the total susceptibility value of larger region approaches to the ideal value more rapidly. This means that by using denser sampling of the dipole field we can quantify iron deposit more precisely in an original resolution.

In the proposed method, latticed pattern artifacts are observed. It is reasonable to infer that the nearest neighbor interpolation method brings the artifacts to measured map and that the artifacts persist in a susceptibility map. These artifacts could be reduced by improving the interpolation method of an input map.

References

[1] J.C. Chen, P.A. Hardy, W. Kucharczyk, M. Clauberg, J.G. Joshi, A. Vourlas, M. Dhar, and R.M. Henkelman, "MR of human postmortem brain tissue: correlative study between T2 and assays of iron and ferritin in Parkinson and Huntington disease., " *Am. J. Neuroradiol,* vol. 14(2), pp.275-281, 1993.

[2] C. Bouras, P. Giannakopoulos, P.F. Good, A. Hsu, P.R. Hof, and D.P. Perl, "A laser microprobe mass analysis of brain aluminum and iron in dementia pugilistica: comparison with Alzheimer's disease., " *Eur. Neurol,* vol. 38, pp. 53-58, 1997

[3] J. P. Marques, and R. Bowtell, "Application of a Fourier-Based Method for Rapid Calculation of Field Inhomogeneity Due to Spatial Variation of Magnetic Susceptibility," *Concepts Magn. Reson. B (Magn. Reson. Eng.)*, vol. 25B, no. 1, pp. 65-78, 2005.

[4] L. de Rochefort, T. Liu, B. Kressler, J. Liu, P. Spincemaille, and Y. Wang, "Quantitative Susceptibility Map Reconstruction from MR Phase Data Using Bayesian Regularization: Validation and Application to Brain Imaging," *Magn. Reson. Med.*, vol. 63, pp. 194-206, 2010.

[5] T. Liu, P. Spincemaille, L. de Rochefort, B. Kressler, and Y. Wang, "Calculation of Susceptibility Through Multiple Orientation Sampling (COSMOS):A Method for Conditioning the Inverse Problem From Measured Magnetic Field Map to Susceptibility Source Image in MRI," *Magn. Reson. Med.*, vol. 61, pp. 196-204, 2009.

[6] S. Wharton, A. Schäfer, and R. Bowtell, "Susceptibility Mapping in the Human Brain Using Threshold- Based k-Space Division," *Magn. Reson. Med.*, vol. 63, pp. 1292-1304, 2010.

[7] M. Murashima, T. Ueno, and N. Sugimoto, "Effective Digitized Spatial Size of Unit Dipole Field in Quantitative Susceptibility Mapping ," in *Proc. 36th EMBC Conf.*, Japan, 2013, pp. 1049-1052.

[8] M. Murashima, T. Ueno, and N. Sugimoto, "Comparisons of Quantitative Susceptibility Mapping (QSM) by using restricted oversampled spatial dipole field, " in *Proc. 21st Annu. Meeting of ISMRM*, Salt Lake City, UT, 2013.

[9] Y. Umemoto, M. Murashima, T. Ueno, and N. Sugimoto, "Resolution improvement in Quantitative Susceptibility Mapping by denser sampling of spatial dipole field, " in *Proc. 22nd Annu. Meeting of ISMRM*, Milan, Italy, 2014.

[10] F. Schweser, A. Deistung, B.W. Lehr, and J.R. Reichenbach, "Quantitative imaging of intrinsic magnetic tissue properties using MRI signal phase: An approach to in vivo brain iron metabolism?," *Neuroimage*, vol. 54, pp. 2789-2807, 2011.